Available online at www.sciencedirect.com
ScienceDirect
Polymer 48 (2007) 3883–3892
polymer
www.elsevier.com/locate/polymer

Calculation of the effect of macromolecular architecture on structure and thermodynamic properties of linear–tri-arm polyethylene blends from Monte Carlo simulation

Anastassia N. Rissanou [a], Loukas D. Peristeras [a,1], Ioannis G. Economou [a,b,*]

[a] National Center for Scientific Research ''Demokritos'', Institute of Physical Chemistry, Molecular Thermodynamics and Modelling of Materials Laboratory, GR – 153 10 Aghia Paraskevi, Attikis, Greece

[b] Technical University of Denmark, Department of Chemical Engineering, IVC-SEP, DK-2800 Lyngby, Denmark

Received 27 February 2007; received in revised form 22 April 2007; accepted 23 April 2007
Available online 3 May 2007

Abstract

A Monte Carlo simulation formalism proposed recently [Peristeras et al. Macromolecules 2007;40:2904–14] is applied here to linear–tri-arm polyethylene blends using atomistic models. Elementary Monte Carlo moves for long chain and branched molecules are used and shown to result in efficient relaxation of long chains. The effect of chain and arm molecular weight and of temperature on the structure and thermodynamic properties of blends is examined. Chemical potential versus composition diagrams are drawn in order to assess the non-ideality of mixing that may lead to phase separation. All of the blends examined are shown to be fully miscible. The microscopic blend structure is examined by calculating the radial distribution function. Finally, the radii of gyration of linear and branched chains are calculated and scaling exponents are evaluated.

Keywords: Polymer thermodynamics; Molecular simulation; Polyolefins

1. Introduction

The study of polyolefin blends is an important and still very challenging problem both scientifically and technologically. Over the last 20 years, numerous studies focused on the elucidation of microscopic structure and the evaluation of macroscopic physical, thermal, mechanical and other properties. A critical parameter in all cases is the miscibility of the polymers that form the blend. A wide range of experimental methods including small-angle neutron scattering [1–11], light scattering [12], transmission electron microscopy [13,14], differential scanning calorimetry [13,14], solid-state NMR [15–17], atomic force microscopy [18] and *PVT* data analysis [19,20] have been used in order to quantify the effect of composition and macromolecular architecture on blend's miscibility. Pressure was also shown to have a considerable effect on the miscibility [19,21].

Theoretical models including Lattice Cluster Theory [22–24] and other lattice equations of state [25–29] have been developed for the description of polyolefin blend's thermodynamic properties and phase behavior as a function of temperature and pressure. At the same time, integral equation theories [30–32] and field theories [33,34] have been used to identify the enthalpic and the entropic effects on polyolefin blend's phase behavior. Molecular simulation is a powerful tool for the elucidation of microscopic structure and prediction of macroscopic polymer properties. In this respect, it has been used for the detailed study of polyolefin blends. In most cases, relatively simple or coarse-grained model systems [35,36] have been employed that maintain the basic chain characteristics. Both Molecular Dynamics (MD) [37–40] and Monte Carlo (MC) [35,36,41–44] simulations have been reported

* Corresponding author. National Center for Scientific Research ''Demokritos'', Institute of Physical Chemistry, Molecular Thermodynamics and Modelling of Materials Laboratory, GR – 153 10 Aghia Paraskevi, Attikis, Greece.
E-mail address: economou@chem.demokritos.gr (I.G. Economou).
[1] Present address: Scienomics, 17 square Edouard VII, 75009 Paris, France.

0032-3861/$ - see front matter © 2007 Elsevier Ltd. All rights reserved.
doi:10.1016/j.polymer.2007.04.066

and compared to integral equation theories. In most cases, good agreement between theory and simulation was obtained.

Molecular simulation with a detailed atomistic representation of macromolecular architecture and explicit account for all intra- and intermolecular interactions is a much more computing time intensive approach. Nevertheless, the realistic representation of polymer molecules makes possible the direct comparison of simulation results with experimental data and, even more important, the interpretation of ambiguous experimental data.

Recently, a semi-grand [*NnPTμ**] statistical ensemble formalism was proposed for blends of linear and branched molecules [45]. In this formalism, the chemical potential difference, $\Delta\mu^*$, between the two components is specified and the blend composition is calculated. Systematic variation of $\Delta\mu^*$ results in different blend compositions, from pure linear polymer to pure branched polymer. A monotonic variation of $\Delta\mu^*$ with composition indicates a fully stable (miscible) system, otherwise the system is unstable (or partially miscible).

The new [*NnPTμ**] formalism is applied here to a number of linear–tri-arm polyethylene blends in order to assess the effect of polymer molecular weight, arm asymmetry, and temperature on the structure and thermodynamic properties of the blends. For the efficient simulation of long polymer molecules, a number of elementary MC moves are employed that include: reptation [46], configuration bias (CB) [47–49], concerted rotation (CONROT) [50,51], flip [52], end-bridging (EB) [51,53], double bridging (DB) [54], branch point flip (BPF) [55], branch point slithering (BPS) [55] and identity-altering (IA) [45]. All these moves result in efficient relaxation of polymer molecules within reasonable computing time while IA allows for mixture composition change in response to $\Delta\mu^*$ value imposed. An accurate united-atom (UA) force field [56,57] is used for the simulation of linear and tri-arm chain molecules. This force field was shown to predict accurately the density of high density polyethylene (corresponding to linear chains here) and low density polyethylene (corresponding to tri-arm chains here) in the melt state over a wide temperature range [55]. In this work, structural and thermodynamic properties of the blends are reported. All of the blends examined are shown to be fully miscible. For some of the blends, a negative excess volume is reported (higher density of the blend compared to pure polymers).

2. System definition and statistical ensemble formalism

The system considered here consists of N_l linear polymer chains and N_b branched polymer chains, so that $N = N_l + N_b$ and $x_b = N_b/N$ is the mole fraction of branched chains. In all cases, the branched chains examined are tri-arm chains (one branch point per chain). The semi-grand [*NnPTμ**] canonical ensemble formalism was presented in detail by Peristeras et al. [45] based on the formalism of Pant and Theodorou [51]. Consequently, only the basic elements of the formalism will be presented here. The probability density function of this ensemble is:

$$\rho^{NnPT\mu^*}(V,\mathbf{r}_1,\mathbf{r}_2,\ldots,\mathbf{r}_n;\text{connectivity}) \propto \exp\left[\beta \sum_{\substack{k=1 \\ k\neq i,j}}^{m} \mu_k^* N_k - \beta PV - \beta u\left(\mathbf{r}_1,\mathbf{r}_2,\ldots,\mathbf{r}_n;\text{connectivity}\right)\right] \tag{1}$$

where T, P, V are the temperature, pressure and volume of the system, $\mathbf{r}_i$ are the spatial coordinates of molecule i, $\beta = 1/k_B T$, μ_k^* is the relative chemical potential of component k and u is the potential energy function. The conformal solution principle is invoked for the configurational integral, so that:

$$Z(V,T,N_1,N_2,\ldots,N_m) = Z(V,T,N,n,N_b) \tag{2}$$

where n is the total number of atoms of the system. According to Eq. (2), the configurational integral depends on the number-averaged molecular weight, density of monomers and mole fraction of branched (or linear) chains but not on the details of the chain length distribution of linear and branched species. This assumption has been shown to be satisfactory for systems of sufficiently long linear polyethylene chains [51]. Eq. (2) allows us to treat our system as a pseudo-binary, consisting of linear and branched chains.

Both linear and branched chains examined here are polydisperse. The range of chain sizes is controlled by setting appropriately the chemical potential values for the different species, so that:

$$\mu_k^* = \begin{cases} 0 & \text{for linear species with a given range of sizes} \\ \mu^* & \text{for tri-arm species with a given range of arm sizes} \\ -\infty & \text{for all other cases} \end{cases} \tag{3}$$

which imposes the same chemical potential for all linear components, and the same relative chemical potential with respect to linear components for all branched components. Obviously, the selection of μ values results in: $\Delta\mu^* = \mu^*_{\text{tri-arm}} - \mu^*_{\text{linear}} = \mu^*$. The ranges of acceptable sizes of linear and branched species need to be specified. A uniform distribution on the size of linear chains and on the size of arms of tri-arm chains is imposed within a pre-selected range of values. This range is defined according to the expression:

$$v_k \in \begin{cases} [\overline{v}_l(1-\Delta_l), \overline{v}_l(1+\Delta_l)] & \text{for linear species} \\ [\overline{v}_q(1-\Delta_q), \overline{v}_q(1+\Delta_q)] & \text{for tri-arm species, } q = 1,2,3 \end{cases} \tag{4}$$

where $\overline{v}_l$ is the mean chain size for linear chains, $\overline{v}_q$ is the mean arm size for arm q of a tri-arm chain, and Δ_l and Δ_q control the range of size for linear chains and for arms of tri-arm chains.

The material balance of the system can be written in terms of the total number of chains and of the total number of atoms [45]. After some cumbersome algebra, the mole fractions of

linear species, x_l, and of branched species, x_b, are obtained [45]:

$$x_l = \frac{2\overline{v}_l \Delta_l + 1}{2\overline{v}_l \Delta_l + 1 + z\exp[\beta\mu^*]\prod_{q=1}^{3}(2\overline{v}_q \Delta_q + 1)} \quad (5)$$

$$x_b = \frac{z\exp[\beta\mu^*]\prod_{q=1}^{3}(2\overline{v}_q \Delta_q + 1)}{2\overline{v}_l \Delta_l + 1 + z\exp[\beta\mu^*]\prod_{q=1}^{3}(2\overline{v}_q \Delta_q + 1)} \quad (6)$$

where z is a measure of the non-ideality of mixing calculated from the expression:

$$z = \exp\left(\left.\frac{\partial \ln(Z)}{\partial N_b}\right|_{V,T,N,n}\right) \quad (7)$$

For an ideal mixture, z assumes a constant value.

In the semi-grand canonical simulations presented here, a range of relative chemical potentials are imposed (Eq. (3)) and, at equilibrium, the system responds with a certain composition value. By re-arranging Eq. (5) or, equivalently, Eq. (6) one may calculate z, and thus assess the non-ideality of the mixture:

$$z = \frac{x_b}{1 - x_b}\frac{2\overline{v}_l \Delta_l + 1}{\exp[\beta\mu^*]\prod_{q=1}^{3}(2\overline{v}_q \Delta_q + 1)} \quad (8)$$

Eq. (8) can be also written as:

$$\beta\mu^* = \ln\left[\frac{2\overline{v}_l \Delta_l + 1}{z\prod_{q=1}^{3}(2\overline{v}_q \Delta_q + 1)}\right] + \ln\left[\frac{x_b}{1 - x_b}\right] \quad (9)$$

For an ideal mixture, the first term on the right hand side of Eq. (9) is constant over the entire μ^*–x_b range of data.

Finally, from the collected μ^*–x_b data, one may assess the system stability. For a stable single-phase mixture, it is [58]:

$$\left.\frac{d\mu^*}{dx_b}\right|_{T,P} \geq 0 \quad (10)$$

3. Systems examined and simulation details

Both linear polyethylene and tri-arm polyethylene were modeled with the TraPPE united-atom (TraPPE-UA) potential [56,57]. TraPPE-UA is a very accurate force field for the calculation of structure and thermodynamic properties of pure *n*-alkanes, branched alkanes, 1-alkenes and other classes of organic compounds and their mixtures. In TraPPE, bond lengths are kept constant. In all cases here, the bond length is 1.54 Å. Bond angle bending is calculated according to the expression:

$$u_{bend} = \frac{1}{2}k_\theta(\theta - \theta_o)^2 \quad (11)$$

whereas for the dihedral torsion angles the following expression is used:

$$u_{tors} = c_0 + c_1[1 + \cos\phi] + c_2[1 - \cos(2\phi)] + c_3[1 + \cos(3\phi)] \quad (12)$$

For the non-bonded intra- and intermolecular interactions the Lennard–Jones potential is used, so that:

$$u_{LJ} = 4\varepsilon\left[\left(\frac{\sigma}{r}\right)^{12} - \left(\frac{\sigma}{r}\right)^{6}\right] \quad (13)$$

The polymers examined here consist of the following three types of UA: CH_2 (the vast majority of groups), CH_3 (terminal groups) and CH (the branch point of tri-arm chains). In Table 1, the force field bonded and non-bonded parameters for the linear and tri-arm chains are shown. For non-bonded interactions between unlike UAs, the Lorentz–Berthelot mixing rules are used:

$$\varepsilon_{ij} = \sqrt{\varepsilon_{ii}\varepsilon_{jj}} \text{ and } \sigma_{ij} = \frac{\sigma_{ii} + \sigma_{jj}}{2} \quad (14)$$

Finally, the Lennard–Jones potential was truncated at $r = 2.5\sigma$ for all types of interactions and tail corrections were applied [59].

Six binary blends of linear polyethylene–tri-arm polyethylene were examined. In Table 2, the characteristics of these blends are specified. Appropriate acronyms are used in order to identify whether the arms of the tri-arm component have the same (symmetric; S) or different (asymmetric; A) sizes and the temperatures. For all blends, the temperature was set

Table 1
TraPPE force field bonded and non-bonded parameters for linear and tri-arm polyethylenes examined in this work

Bond angle		Θ_0		k_θ/k_B [K]
CH_x–(CH_2)–CH_y		114		62 500
CH_x–(CH)–CH_y		112		62 500
Dihedral angle	c_0/k_B [K]	c_1/k_B [K]	c_2/k_B [K]	c_3/k_B [K]
CH_x–(CH_2)–(CH_2)–CH_y	0	335.03	−68.19	791.32
CH_x–(CH_2)–(CH)–CH_y	−251.06	428.73	−111.85	441.27
UA		ε/k_B [K]		σ [Å]
CH_3		98		3.75
CH_2		46		3.95
CH		10		4.68

Table 2
Binary linear polyethylene–tri-arm polyethylene blends examined in this work

Blend acronym	T (K)	P (MPa)	Linear PE	Branched PE
B1S450	450	0.1	C_{121}	$(C_{40})_3$
B1S350	350	0.1	C_{121}	$(C_{40})_3$
B1A450	450	0.1	C_{121}	$C_{30} \times C_{30} \times C_{60}$
B2S450	450	0.1	C_{301}	$(C_{100})_3$
B2A450	450	0.1	C_{301}	$C_{20} \times C_{20} \times C_{260}$
B3S450	450	0.1	C_{601}	$(C_{200})_3$

equal to 450 K while for blend B1 a lower temperature of 350 K was also examined. In all cases, pressure was set constant at 0.1 MPa. Furthermore, the relative chemical potential values, $\beta\mu^*$, varied in the range (−15 to 25) k_BT. Both linear and tri-arm polymers were polydisperse with a uniform molecular weight distribution as imposed by Eqs. (3) and (4). Δ_l and Δ_q that characterize the range of linear chain and arm sizes (Eq. (4)), respectively, were set equal to 0.5 in all cases. The total number of chains N and total number of atoms n in every system simulated were set constant. In all cases, n varied between 4500 and 4850 and N was adjusted accordingly.

The frequency of elementary MC moves in a typical simulation was: 10% reptation, 4% end-rotation, 10% CONROT, 10% re-bridging, 24.5% EB, 0.5% volume fluctuation, 3% dimer flip, 4% BPS, 4% BPF and 30% IA. For the blend B4S450 where the sizes of linear and branched chains differ substantially the acceptance ratio of the IA is lower than that for the other blends. In this case, the fraction of IA attempted moves increases to 38%. A typical run consisted of 10^8–2×10^8 MC moves of which the first 5×10^7 were used for system equilibration and the remaining for averaging and calculating structure and thermodynamic properties.

4. Results and discussion

Simulation results will be presented and discussed for groups of blends so that a systematic analysis of the effect of macromolecular characteristics and temperature on the thermodynamic and structural properties is possible.

4.1. B1 blends

These blends (B1S450, B1S350 and B1A450) consist of the same linear polyethylene (C_{121}). In Fig. 1, the composition (x_b)–relative chemical potential ($\beta\mu^*$) plot is shown for B1S450 and B1A450 blends. Both blends are stable over the entire composition range (complete miscibility). Furthermore, the asymmetry of the tri-arm polyethylene in the second blend has very little effect on this diagram. The solid curves correspond to Eq. (9) assuming a constant z value for different blend compositions that results in a constant value for the first term of the right hand side of the equation. For B1S450, the solid curve is given from the expression:

$$\beta\mu^*_{\mathrm{B1S450}} = 0.5 + \ln\left[\frac{x_b}{1-x_b}\right] \tag{15}$$

while for B1A450 from the expression:

$$\beta\mu^*_{\mathrm{B1A450}} = 0.66 + \ln\left[\frac{x_b}{1-x_b}\right] \tag{16}$$

If one assumes that $z_{\mathrm{B1S450}} = z_{\mathrm{B1A450}}$ and applies Eq. (9) for the two blends then one gets:

$$\begin{aligned}\beta\mu^*_{\mathrm{B1S450}} - \beta\mu^*_{\mathrm{B1A450}} &= \ln\left[\frac{2\times120\times0.5+1}{z_{\mathrm{B1S450}}(2\times40\times0.5+1)^3}\right] \\ &\quad - \ln\left[\frac{2\times120\times0.5+1}{z_{\mathrm{B1S450}}(2\times30\times0.5+1)^2(2\times60\times0.5+1)}\right] \\ &= -0.16\end{aligned} \tag{17}$$

which agrees exactly with the difference predicted by Eqs. (15) and (16). In other words, the difference in the macromolecular architecture of the branched chains of the two blends has no effect on z.

Attention is further focused on the microscopic structure of the two blends for $\beta\mu^* = 1$ that corresponds to $x_b = 0.60 \pm 0.07$ for B1S450 and 0.56 ± 0.09 for B1A450. Intermolecular pair radial distribution function, $g(r)$, provides a reliable picture of the microscopic structure of polymer blends. In Fig. 2, MC simulation results are presented for the $g(r)$ of CH_2–CH_2 interactions for B1S450 and B1A450. For the blends examined, CH_2–CH_2 is by far the most important

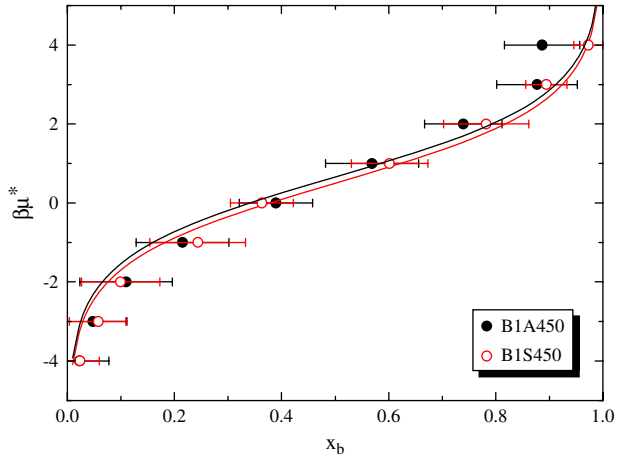

Fig. 1. The relative chemical potential, $\beta\mu^*$, as a function of composition, x_b, for blends B1S450 and B1A450. Solid curves correspond to Eqs. (15) and (16), respectively.

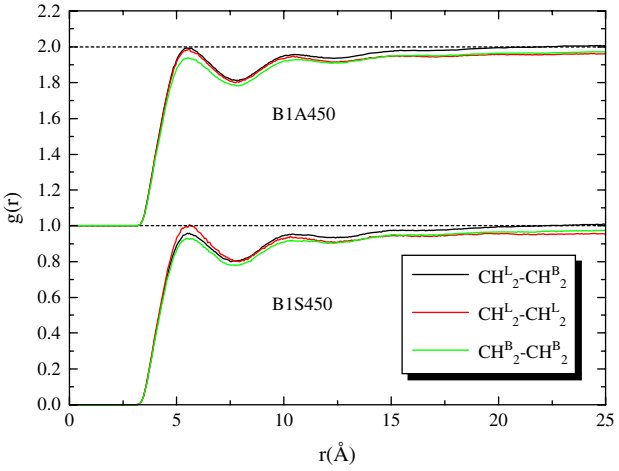

Fig. 2. Radial distribution function, $g(r)$, for CH_2–CH_2 interactions of B1S450 at $x_b = 0.60 \pm 0.07$ and B1A450 at $x_b = 0.56 \pm 0.09$ blends.

type of interactions. For the B1S450 blend, $g(r)$ for $CH_2^L-CH_2^L$ exhibits the highest peak value followed by the $g(r)$ for the cross-interaction between linear and branched chains, $CH_2^L-CH_2^B$. For the case of B1A450 blend, $g(r)$ for $CH_2^L-CH_2^L$ and $CH_2^L-CH_2^B$ is very similar concerning the position and height of the first peak while at larger distances unlike interactions $CH_2^L-CH_2^B$ seem to result in a higher $g(r)$ value. In both blends as well as the rest of the blends examined here, $g(r)$ for $CH_2^B-CH_2^B$ assumes the lowest value at relatively short distances. This is a manifestation that branched chains have a more dense globular structure excluding other branched chains from their immediate vicinity. Finally, all $g(r)$ have a value lower than one over an extended range of distances, due to the 'correlation hole effect' that has been observed also by Theodorou and co-workers for other polymer systems [53,60,61].

For both blends, all four different $g(r)$ for CH_3-CH_2 interactions are very similar to each other (not shown here). The CH_3-CH_2 pairs exhibit a higher first peak value compared to CH_2-CH_2 pairs as expected, because of the corresponding higher Lennard–Jones energy parameter, that is, $\varepsilon_{CH_3-CH_2}/k_B = 67.1$ K and $\varepsilon_{CH_2-CH_2}/k_B = 46$ K.

An additional quantity that characterizes the microscopic structure of polyethylene blends is the structure factor, $S(q)$. Structure factor corresponds to the Fourier transform of the total pair distribution function, i.e. the sum of all intra- and intermolecular $g(r)$. In Fig. 3, $S(q)$ for both B1S450 and B1A450 is shown. Results for the two systems practically coincide.

In Fig. 4, the mean square radius of gyration, $\langle R_g^2\rangle$, is shown as a function of carbon number of linear and tri-arm polyethylenes for the two blends at a given $\beta\mu^*$ value. In both cases, tri-arm molecules form more compact structures than the linear molecules of the same size, and thus $\langle R_g^2\rangle_b$ is always smaller than $\langle R_g^2\rangle_l$. This supports further the calculations for $g(r)$ discussed above. Based on detailed geometrical analysis, Zimm and Stockmayer [62] developed a theoretical method for the calculation of the ratio $g = \langle R_g^2\rangle_b/\langle R_g^2\rangle_l$ for unperturbed

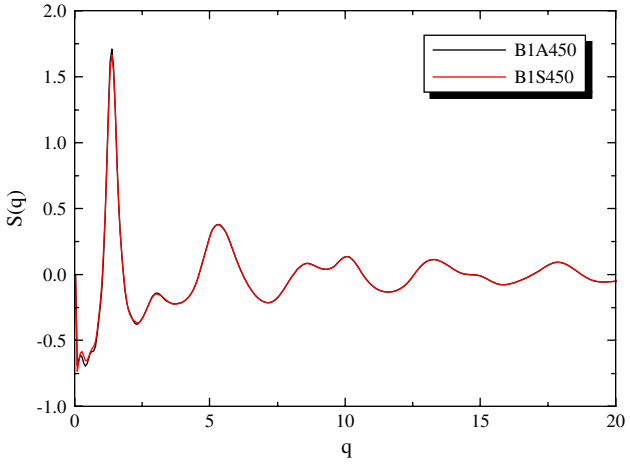

Fig. 3. Structure factor, $S(q)$, for B1S450 at $x_b = 0.60 \pm 0.07$ and B1A450 at $x_b = 0.56 \pm 0.09$ blends from molecular simulation.

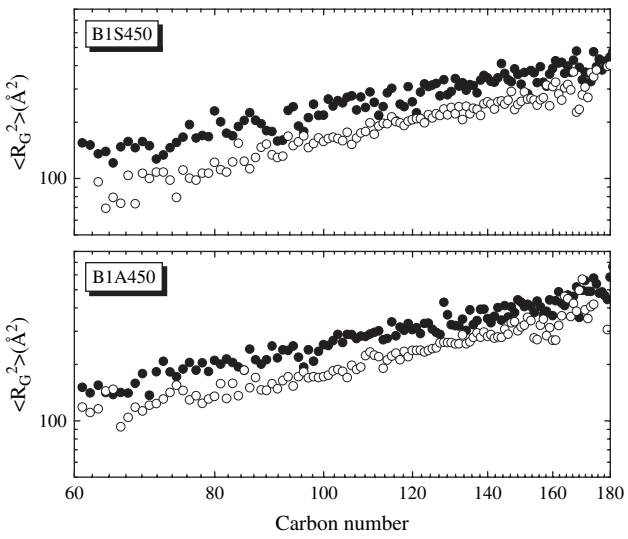

Fig. 4. Mean square radius of gyration, $\langle R_g^2\rangle$, as a function of carbon number for the linear (dark symbols) and tri-arm (open symbols) molecules for (top) B1S450 at $x_b = 0.60 \pm 0.07$ and (bottom) B1A450 at $x_b = 0.56 \pm 0.09$ blends.

branched and linear chains of same size. Appropriate expressions were proposed for symmetric and asymmetric branched chains of variable functionality (number of branches attached to a branch point). In Table 3, g values calculated from the simulations performed here for a particular $\beta\mu^*$ value that corresponds to a certain composition and from Zimm and Stockmayer theory are reported. For the B1 blends at 450 K, simulation results are 5–6% below the theoretical predictions. For the B1S350 blend, the deviation between theory and simulation is higher, probably because the chain dimensions are not fully equilibrated.

For the root mean square radius of gyration of polymer chains, the following scaling equation holds [63]:

$$\left\langle R_g^2\right\rangle^{1/2} \sim X^v \tag{18}$$

where X is the number of carbon atoms in the polymer and v is 0.5 for the case of unperturbed chains and 0.6 for the case of good solvent conditions. In general, polymer melts for sufficiently high X exhibit unperturbed chain behavior. From the simulation data presented in Fig. 4, the v values obtained are shown in Table 3. In all cases, v is higher than 0.5. For the tri-arm chains especially, v assumes a value higher than good solvent conditions, indicating that the size of the arms is not high enough so that the chain sizes behave as random walks.

MC simulations in the semi-grand ensemble for B1S blend were performed also at 350 K. Such a lower temperature is considerably more demanding in terms of computing time in order to achieve relaxation of long polymer chains. The ability of the elementary MC moves used here to equilibrate the system is initially assessed. The autocorrelation function, $\langle \hat{\mathbf{v}}_{ee}(0)\cdot\hat{\mathbf{v}}_{ee}(i)\rangle$, for the end-to-end unit vector of the linear chains and of the arm end-to-arm end unit vector of the tri-arm

Table 3
$g = \langle R_g^2\rangle_b/\langle R_g^2\rangle_l$ values from molecular simulation and Zimm–Stockmayer [62] theory and exponent ν in Eq. (18) based on MC simulations for the binary linear polyethylene–tri-arm polyethylene blends examined

Blend	x_b	$g = \langle R_g^2\rangle_b/\langle R_g^2\rangle_l$		ν	
		Simulation	Theory [62]	Linear	Tri-arm
B1S450	0.60 ± 0.07	0.73 ± 0.12	0.778	0.54 ± 0.02	0.67 ± 0.02
B1S350	0.26 ± 0.06	0.68 ± 0.12	0.778	0.59 ± 0.01	0.69 ± 0.03
B1A450	0.56 ± 0.09	0.77 ± 0.17	0.813	0.58 ± 0.01	0.63 ± 0.01
B2S450	0.55 ± 0.11	0.73 ± 0.18	0.778	0.58 ± 0.02	0.52 ± 0.02
B2A450	0.63 ± 0.08	0.94 ± 0.37	0.964	0.53 ± 0.02	0.59 ± 0.03
B3S450	0.62 ± 0.18	0.85 ± 0.31	0.778	0.55 ± 0.02	0.48 ± 0.02

chains at 350 K and $x_b = 0.26 \pm 0.06$ is shown in Fig. 5. Very long simulations, in the order of 100 million MC moves, are needed so that $\langle \hat{\mathbf{v}}_{ee}(0) \cdot \hat{\mathbf{v}}_{ee}(i) \rangle$ achieves values close to zero that indicate long chain relaxation. For comparison, calculations at 450 K are also shown. At this higher temperature, chain relaxation is achieved within 20 million MC steps.

The composition (x_b)–relative chemical potential ($\beta\mu^*$) simulation results for B1S350 are shown in Fig. 6. For comparison, results for B1S450 are also shown. A monotonic change of composition is obtained in response to increase of $\beta\mu^*$, which indicates a fully stable system. However, compared to the same blend at 450 K, a flattening of the hypothetical curve drawn through the data is observed at intermediate compositions. As a result, the fit of Eq. (9) with $z =$ constant is not sufficient and a variable z is needed for an accurate correlation. This indicates that as temperature decreases the mixture becomes progressively non-ideal. At sufficiently lower temperatures, one may expect this non-ideality to result in macro-phase separation (UCST behavior).

The intermolecular $g(r)$ functions for the various CH_3–CH_2 and CH_2–CH_2 pairs of B1S350 are shown in Fig. 7 at $\beta\mu^* = 1.0$ that corresponds to $x_b = 0.26 \pm 0.06$. The b–b interaction is substantially lower for both pairs which can be attributed to more intramolecular packed structure of the tri-arm chains compared to linear chains. This argument is further supported by a relatively lower g value of 0.68 ± 0.12 for this blend. The difference in $g(r)$ between the various pairs is more significant at 350 K compared to 450 K (Fig. 2). Here again the 'correlation hole effect' is shown to be important, especially for the b–b interaction.

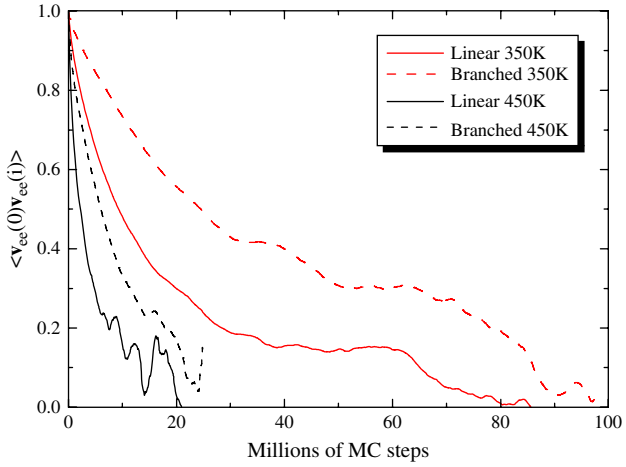

Fig. 5. Relaxation of the end-to-end unit vector of linear chains and of the arm end-to-arm end unit vector of tri-arm chains for B1S350 and B1S450 blends.

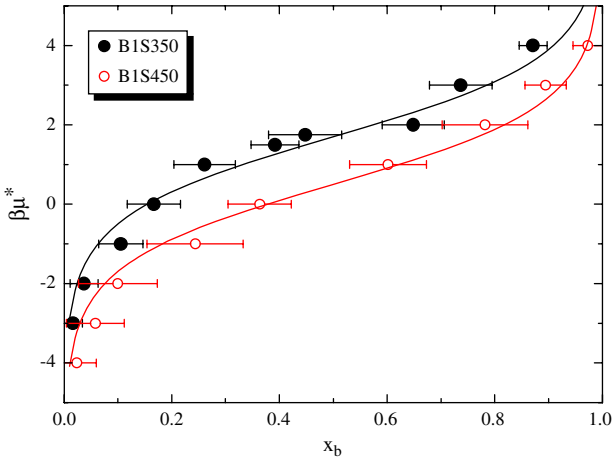

Fig. 6. The relative chemical potential, $\beta\mu^*$, as a function of composition, x_b, for blends B1S350 and B1S450. Points are simulation results and solid lines correspond to the following expressions: $\beta\mu^*_{B1S350} = 1.7 + \ln[x_b/(1-x_b)]$ and $\beta\mu^*_{B1S350} = 0.5 + \ln[x_b/(1-x_b)]$.

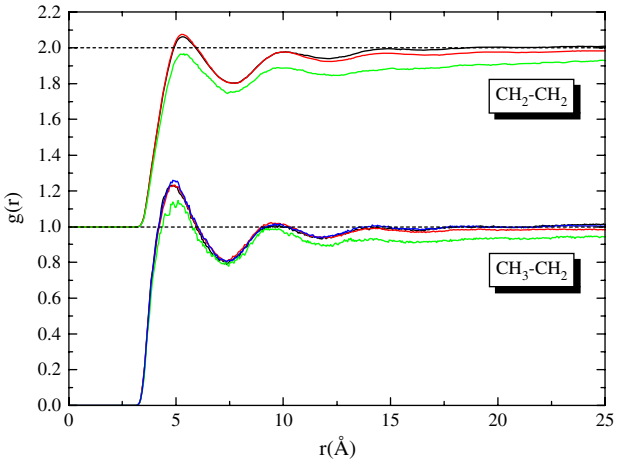

Fig. 7. Radial distribution function for CH_2–CH_2 and CH_3–CH_2 pairs of B1S350 at $x_b = 0.26 \pm 0.06$. Black line: linear–branched, red line: linear–linear, green line: branched–branched, blue line: branched–linear for the case of CH_3–CH_2. (For interpretation of the references to color in this figure legend, the reader is referred to the web version of this article.)

4.2. B2 blends

The two blends examined here are a blend where the tri-arm component consists of three equal size arms (B2S450) and a blend where the tri-arm component is highly asymmetric (B2A450), so that one arm is 13 times longer than the other two, i.e. C_{260} versus C_{20}. In Fig. 8, the x_b–$\beta\mu^*$ simulation data for the two blends are presented. Both blends are fully miscible and exhibit an almost ideal mixing behavior. Eq. (9) with a constant z value results in a good fit of the data. Furthermore, if one assumes that z is the same for the two blends, then one may calculate the expected offset between the two curves from Eq. (9). It is:

$$\begin{aligned}\beta\mu^*_{\mathrm{B2S450}} - \beta\mu^*_{\mathrm{B2A450}} &= \ln\left[\frac{2\times 300\times 0.5+1}{z(2\times 100\times 0.5+1)^3}\right] \\ &\quad - \ln\left[\frac{2\times 300\times 0.5+1}{z(2\times 20\times 0.5+1)^2(2\times 260\times 0.5+1)}\right] \\ &= -2.2 \end{aligned} \tag{19}$$

The actual offset predicted by the best fits of the simulation data turns out to be $\beta\mu^*_{\mathrm{B2S450}} - \beta\mu^*_{\mathrm{B2A450}} = -2.5$. This relatively small difference may be attributed to the statistical uncertainty of the simulation results (expressed in Fig. 8 as uncertainty in the equilibrium composition) and/or some dependence of z from the molecular weight of chains examined.

The mass density of B2A450 blend was calculated from the semi-grand simulations and is presented in Fig. 9a, as a function of composition. The two pure polymer melts have similar densities at 450 K, as measured experimentally and predicted by TraPPE force field [55]. For all compositions, blend density is higher compared to either of the two pure polymers indicating that the blends examined assume negative excess volume values. Such behavior agrees with lattice model predictions

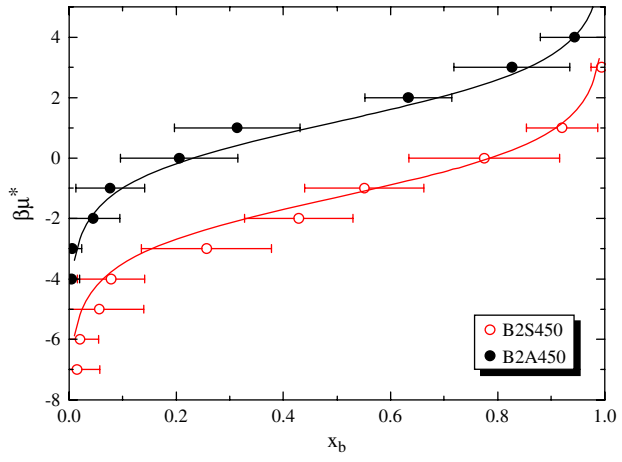

Fig. 8. The relative chemical potential, $\beta\mu^*$, as a function of composition, x_b, for blends B2S450 and B2A450. Points are simulation results and solid lines correspond to the following expressions: $\beta\mu^*_{\mathrm{B2S450}} = -1.3 + \ln[x_b/(1-x_b)]$ and $\beta\mu^*_{\mathrm{B2A450}} = 1.2 + \ln[x_b/(1-x_b)]$.

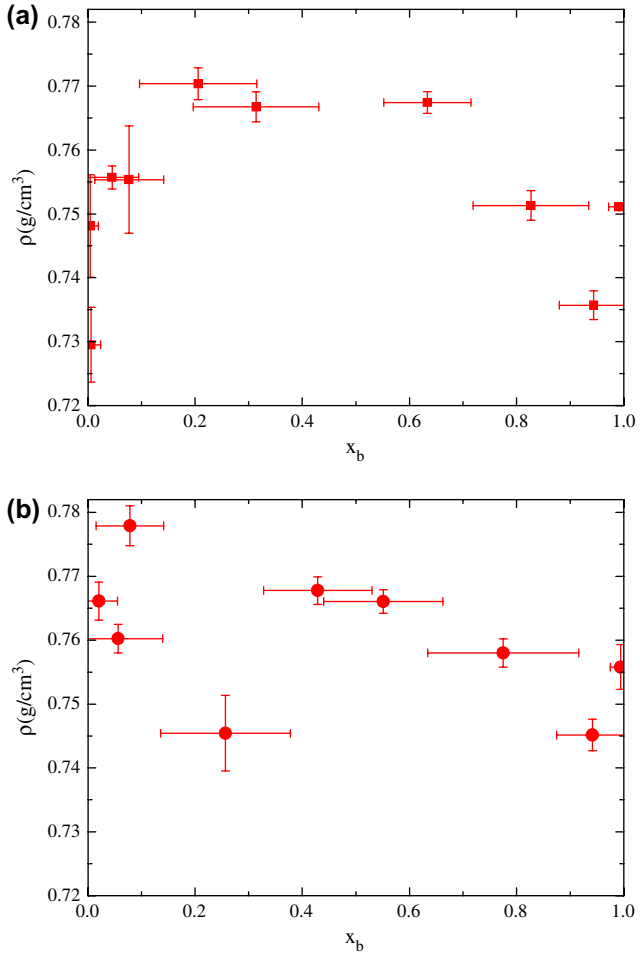

Fig. 9. Mass density of (a) B2A450 and (b) B2S450 blends as a function of composition.

for poly(ethylene-*alt*-propylene) – head-to-head polypropylene blends [27] and with Monte Carlo simulations on model polyethylene blends [64]. As a result, one may conclude that pressure is expected to have a substantial effect on the mixing properties of this blend. For the case of B2S450 blend (Fig. 9b), the variation of density with composition is less pronounced and the excess volume exhibits significant scatter. In Fig. 9, statistical error is reported both for composition and for density. This is a consequence of the semi-grand statistical ensemble where simulations are performed and for which the chemical potential is specified rather than the composition. The magnitude of the statistical error in the composition can be attributed also to the relatively small number of linear and tri-arm chains in the blend (32 in total) that result in larger fluctuations in composition as a result of successful IA moves.

Radial intermolecular distribution functions for the different CH_2–CH_2 pairs for the two B2 blends are shown in Fig. 10. Interactions between unlike CH_2 groups are much stronger than that between like groups, especially for the B2S450 blend. This is in agreement with the higher density at intermediate compositions reported in Fig. 9. At large distances, $g(r)$ for CH_2^{L}–CH_2^{B} approaches unity much faster than $g(r)$ for the other two pairs for both blends. In the case

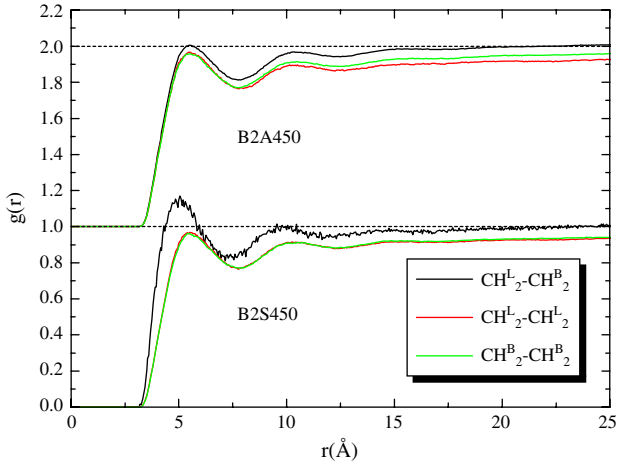

Fig. 10. Radial distribution function, $g(r)$, for CH_2–CH_2 pairs of B2S450 at $x_b = 0.55 \pm 0.11$ and B2A450 at $x_b = 0.63 \pm 0.08$ blends.

of CH_3–CH_2, $g(r)$ for all four pairs is very close to each other (not shown here).

In Fig. 11a and b, $\langle R_g^2 \rangle$ as a function of carbon number is shown for linear and tri-arm chains for B2S450 and B2A450, respectively. The corresponding g values are reported in Table 3. Because of its two relatively short branches, the tri-arm polymer in B2A450 blend exhibits structural characteristics that resemble the linear polymer and assumes $\langle R_g^2 \rangle$ values that are very close to the values of the corresponding linear polymer. Furthermore, exponent ν assumes values in the range 0.5–0.6 in all cases (see Table 3). This indicates that B2 blends with a higher chain length compared to B1 blends can be described by the scaling law of Eq. (18).

4.3. B3 blend

A single B3 blend was examined here consisting of a long linear polyethylene (C_{601}) and a symmetric tri-arm polyethylene (three C_{200} arms). Here again, a monotonic variation of composition (x_b) with the relative chemical potential ($\beta\mu^*$) was obtained (see Fig. 12). Because of the relatively small number of chains in the simulation box, composition exhibits larger fluctuations compared to previous blends. Eq. (9) with a constant z value is able to correlate simulation data accurately. For comparison, simulation results for B1S450 and B2S450 are also shown. By assuming the same z value for all three blends, theoretical offsets can be calculated for the three different pairs of blends based simply on chain characteristics. It is:

$$\beta\mu^*_{B1S450} - \beta\mu^*_{B2S450} = \ln\left[\frac{2\times 120\times 0.5+1}{z(2\times 40\times 0.5+1)^3}\right] - \ln\left[\frac{2\times 300\times 0.5+1}{z(2\times 100\times 0.5+1)^3}\right] = 1.8 \quad (20)$$

$$\beta\mu^*_{B1S450} - \beta\mu^*_{B3S450} = \ln\left[\frac{2\times 120\times 0.5+1}{z(2\times 40\times 0.5+1)^3}\right] - \ln\left[\frac{2\times 600\times 0.5+1}{z(2\times 200\times 0.5+1)^3}\right] = 3.2 \quad (21)$$

$$\beta\mu^*_{B2S450} - \beta\mu^*_{B3S450} = \ln\left[\frac{2\times 300\times 0.5+1}{z(2\times 100\times 0.5+1)^3}\right] - \ln\left[\frac{2\times 600\times 0.5+1}{z(2\times 200\times 0.5+1)^3}\right] = 1.4 \quad (22)$$

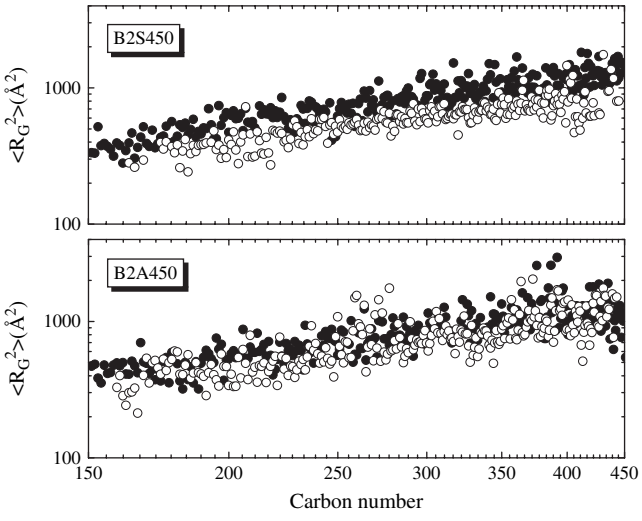

Fig. 11. Mean square radius of gyration, $\langle R_g^2 \rangle$, as a function of carbon number for the linear (dark symbols) and tri-arm (open symbols) molecules of (a) B2S450 blend at $x_b = 0.55 \pm 0.11$ and (b) B2A450 blend at $x_b = 0.63 \pm 0.08$.

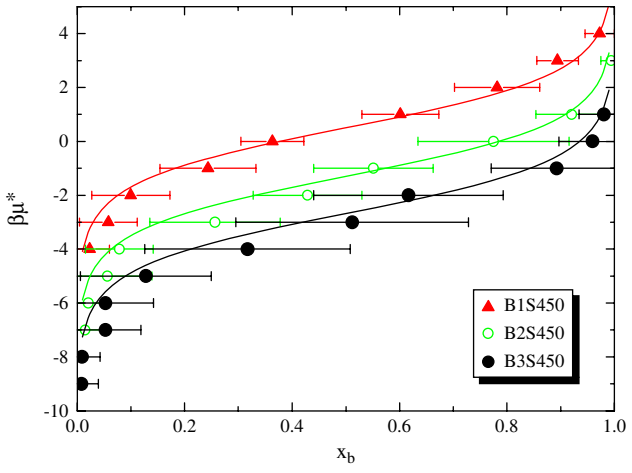

Fig. 12. The relative chemical potential, $\beta\mu^*$, as a function of composition, x_b, for blends B1S450, B2S450 and B3S450. Points are simulation results and solid lines correspond to the fit of Eq. (9). For B3S450, it is: $\beta\mu^*_{B3S450} = -2.7 + \ln[x_b/(1-x_b)]$.

Interestingly, all three theoretical values agree fully with the values calculated from the fits of Eq. (9), indicating that z remains unchanged for different molecular weight values of the linear and tri-arm polyethylenes.

Simulation results for B3S450 blend revealed negative excess volume values, similar to the one reported for B2 blends. The g value predicted for this blend is higher than the theoretical value but the error bar is large (see Table 3), and so no final conclusions can be drawn. Finally, the ν exponent, especially for the tri-arm chains, approaches unperturbed chain conditions indicating that the arm length of 200 is sufficient now for the scaling law to be satisfied.

5. Conclusions

Polyethylene blend miscibility is affected greatly by the macromolecular chain architecture and the molecular weight of the constituent polymers. In addition, temperature and pressure influence the phase behavior of such systems. In this work, binary polyethylene blends consisted of linear and tri-arm chains were examined using a newly proposed semi-grand ensemble MC simulation scheme. Elementary MC moves that result in efficient relaxation of long chain molecules were utilized. The effect of chain size, of arm size and of branched chain asymmetry in terms of arm sizes was examined. All simulations were performed at 0.1 MPa and 450 K while for B1 blend simulations were performed also at 350 K. All blends were found fully miscible while increased non-ideal mixing effects were detected for the B1 blend at 350 K.

B2 and B3 blends examined exhibit negative excess volume which has been reported previously for real polyolefin blends from a lattice macroscopic model and for model polyolefin blends from Monte Carlo simulations. The radial distribution functions reported for these blends, further support the argument that unlike interactions are stronger than like interactions.

Finally, the radii of gyrations of linear and tri-arm chains were calculated and the scaling exponent ν that characterizes the chain size effect was evaluated. For the linear chains, ν was calculated a little higher than 1/2. For the tri-arm chains, the estimated value was in the region of unperturbed chain conditions for high arm lengths (for the B3 blend), in good solvent conditions for intermediate arm lengths (for the B2 blends) and higher than 0.6 (for the B1 blends), which questions the validity of the scaling law for low arm length values (below 40).

Acknowledgments

Professor Doros N. Theodorou, National Technical University of Athens, Greece is gratefully acknowledged for many discussions and recommendations regarding this work and for critically reading the manuscript. Financial support was provided by the General Secretariat of Research and Technology, Greece through the *Collaborative Research Projects with Third Countries* (*project no. HΠA-010*) program to I.G.E. I.G.E. is thankful to the Technical University of Denmark, Department of Chemical Engineering, IVC-SEP for a visiting professorship funded by the Danish Research Council for Technology and Production Sciences (project: *Development and Validation of Computational Tools for Soft Material Structure and Properties,* project coordinator: Associate Professor Georgios Kontogeorgis).

References

[1] Bates FS, Wignall GD, Koehler WC. Phys Rev Lett 1985;55:2425.
[2] Jinnai H, Hasegawa H, Hashimoto T, Han CC. J Chem Phys 1993; 99:4845.
[3] Banaszak M, Petsche IB, Radosz M. Macromolecules 1993;26:391.
[4] Graessley WW, Krishnamoorti R, Balsara NP, Butera RJ, Fetters LJ, Lohse DJ, et al. Macromolecules 1994;27:3896.
[5] Krishnamoorti R, Graessley WW, Balsara NP, Lohse DJ. Macromolecules 1994;27:3073.
[6] Krishnamoorti R, Graessley WW, Fetters LJ, Garner RT, Lohse DJ. Macromolecules 1995;28:1252.
[7] Graessley WW, Krishnamoorti R, Reichart GC, Balsara NP, Fetters LJ, Lohse DJ. Macromolecules 1995;28:1260.
[8] Krishnamoorti R, Graessley WW, Dee GT, Walsh DJ, Fetters LJ, Lohse DJ. Macromolecules 1996;29:367.
[9] Hammouda B, Balsara NP, Lefebvre AA. Macromolecules 1997;30: 5572.
[10] Reichart GC, Graessley WW, Register RA, Krishnamoorti R, Lohse DJ. Macromolecules 1997;30:3363.
[11] Jeon HS, Lee JH, Balsara NP, Newstein MC. Macromolecules 1998; 31:3340.
[12] Bates FS, Wiltzius P. J Chem Phys 1989;91:3258.
[13] Hill MJ, Barham PJ. Polymer 1995;36:1523.
[14] Schipp C, Hill MJ, Barham PJ, Cloke VM, Higgins JS, Oiarzabal L. Polymer 1996;37:2291.
[15] White JL, Brant P. Macromolecules 1998;31:5424.
[16] White JL, Lohse DJ. Macromolecules 1999;32:958.
[17] Wolak J, Jia X, Gracz H, Stejskal EO, White JL, Wachowicz M, et al. Macromolecules 2003;36:4844.
[18] Stephens CH, Hiltner A, Baer E. Macromolecules 2003;36:2733.
[19] Rabeony M, Lohse DJ, Garner RT, Han SJ, Graessley WW, Migler KB. Macromolecules 1998;31:6511.
[20] Han SJ, Lohse DJ, Condo PD, Sperling LH. J Polym Sci Polym Phys 1999;37:2835.
[21] Lefebvre AA, Lee JH, Balsara NP, Hammouda B, Krishnamoorti R, Kumar S. Macromolecules 1999;32:5460.
[22] Dudowicz J, Freed KF. Macromolecules 1995;28:6625.
[23] Freed KF, Dudowicz J. Macromolecules 1996;29:625.
[24] Freed KF, Dudowicz J. Macromolecules 1998;31:6681.
[25] Kumar SK, Veytsman BA, Maranas JK, Crist B. Phys Rev Lett 1997;79:2265.
[26] Luettmer-Strathmann J, Lipson JEG. Macromolecules 1999;32:1093.
[27] Lipson JEG, Tambasco M, Willets KA, Higgins JS. Macromolecules 2003;36:2977.
[28] Vanhee S, Koningsveld R, Berghmans H, Šolc K, Stockmayer WH. Macromolecules 2000;33:3924.
[29] Economou IG. Macromolecules 2000;33:4954.
[30] Weinhold JD, Kumar SK, Singh C, Schweizer KS. J Chem Phys 1995;103:9460.
[31] Rajasekaran JL, Curro JG, Honeycutt JD. Macromolecules 1995; 28:6843.
[32] Singh C, Schweizer KS. Macromolecules 1997;30:1490.
[33] Bates FS, Fredrickson GH. Macromolecules 1994;27:1065.
[34] Fredrickson GH, Liu AJ, Bates FS. Macromolecules 1994;27:2503.
[35] Kacker N, Weinhold JD, Kumar SK. J Chem Soc Faraday Trans 1995;91:2457.
[36] Kumar SK, Weinhold JD. Phys Rev Lett 1996;77:1512.

[37] Stevenson CS, Curro JG, McCoy JD, Plimpton SJ. J Chem Phys 1995;103:1208.
[38] Maranas JK, Mondello M, Grest GS, Kumar SK, Debenedetti PG, Graessley WW. Macromolecules 1998;31:6991.
[39] Maranas JK, Kumar SK, Debenedetti PG, Graessley WW, Mondello M, Grest GS. Macromolecules 1998;31:6998.
[40] Choi P. Polymer 2000;41:8741.
[41] Müller M, Binder K. Macromolecules 1995;28:1825.
[42] Müller M. Macromolecules 1995;28:6556.
[43] Rouault Y, Borisov OV. Macromolecules 1996;29:2605.
[44] Xu G, Clancy TC, Mattice WL, Kumar SK. Macromolecules 2002; 35:3309.
[45] Peristeras LD, Rissanou AN, Economou IG, Theodorou DN. Macromolecules 2007;40:2904.
[46] Vacatello M, Avitabile G, Corradini P, Tuzi A. J Chem Phys 1980; 73:548.
[47] Frenkel D, Mooij GCAM, Smit B. J Phys Condens Matter 1992; 4:3053.
[48] Siepmann JI, Frenkel D. Mol Phys 1992;75:59.
[49] de Pablo JJ, Laso M, Siepmann JI, Suter UW. Mol Phys 1993;80:55.
[50] Dodd LR, Boone TD, Theodorou DN. Mol Phys 1993;78:961.
[51] Pant PVK, Theodorou DN. Macromolecules 1995;28:7224.
[52] Mavrantzas VG, Theodorou DN. Macromolecules 1998;31:6310.
[53] Mavrantzas VG, Boone TD, Zervopoulou E, Theodorou DN. Macromolecules 1999;32:5072.
[54] Karayiannis NCh, Mavrantzas VG, Theodorou DN. Phys Rev Lett 2002;88:105503.
[55] Peristeras LD, Economou IG, Theodorou DN. Macromolecules 2005; 38:386.
[56] Martin MG, Siepmann JI. J Phys Chem B 1998;102:2569.
[57] Martin MG, Siepmann JI. J Phys Chem B 1999;103:4508.
[58] Modell M, Reid RC. Thermodynamics and its applications. Prentice-Hall; 1983.
[59] Allen MP, Tildesley DJ. Computer simulation of liquids. Oxford University Press; 1987.
[60] Doxastakis M, Mavrantzas VG, Theodorou DN. J Chem Phys 2001; 115:11339.
[61] Logotheti GE, Theodorou DN. Macromolecules 2007;40:2235.
[62] Zimm BH, Stockmayer WH. J Chem Phys 1949;17:1301.
[63] de Gennes P-G. Scaling concepts in polymer physics. Cornell University Press; 1979.
[64] Beiner M, Fytas G, Meier G, Kumar SK. Phys Rev Lett 1998;81:594.